INVERSE PROBLEMS IN ENGINEERING MECHANICS
M. Tanaka, G.S. Dulikravich (Eds.)

FOURIER SERIES SOLUTION FOR INVERSE DESIGN OF AERODYNAMIC SHAPES

G. S. DULIKRAVICH and D. P. BAKER
Department of Aerospace Engineering, The Pennsylvania State University
University Park, PA 16802, U.S.A.

ABSTRACT

A new formulation based on the Fourier series has been developed for the inverse design of aerodynamic shapes subject to a specified surface pressure distribution. The method is analytical and can be used in conjunction with any available flow-field analysis code without a need for modification of such a code. The new method was found to converge quickly and at a similar rate for both symmetric (non-lifting) and asymmetric (lifting) aerodynamic shapes and with either a potential flow solver, an Euler flow solver, or a Navier-Stokes flow solver.

KEYWORDS

Shape design, aerodynamics, Fourier series, convergence rates.

INTRODUCTION

Aerodynamic shape inverse design methods have a goal of determining the proper shape of an aerodynamic body that will generate the desired (target) pressure distribution on the surface of such a body. There are many methods [1,2,3] that are capable of such inverse determination of domain size and shape. Most of these methods require the development of new complex mathematical formulations and the accompanying new software. Therefore, inverse shape design methods that require a minimum of software development and which can accept any existing reliable flow-field analysis computer code, unmodified as an interchangeable large subroutine, are highly desirable.

Probably the simplest such method for the inverse design of aerodynamic shapes is the elastic surface membrane concept first proposed by Garabedian and McFadden [4] who considered the surface of an aerodynamic body to deform under aerodynamic loads in a manner similar to an elastic membrane. Their method was then adapted by Malone [5,6] into what is now known as the MGM (modified Garabedian-McFadden or Malone-Garabedian-McFadden) technique.

In order to clarify the main topic of this paper, it will be helpful to first explain the basic MGM concept as applied to inverse design of an airfoil shape subject to a desired distribution of surface pressure. The classic MGM procedure of inverse shape design follows the equation

$$\beta_0 \Delta y + \beta_1 \frac{d\Delta y}{dx} + \beta_2 \frac{d^2 \Delta y}{dx^2} = \Delta C_p \qquad (1)$$

where ΔC_p is the difference between the desired (target) coefficient of surface pressure distribution and the computed coefficient of surface pressure distribution on a guessed airfoil shape. Traditionally, (1) is solved for the correction in airfoil y-coordinates (Δy) by discretizing the airfoil contour line and utilizing finite differencing at each discretization point i on that contour to represent the first derivative and the second derivative in (1). The result is a set of linear algebraic equations of the form

$$A_i \Delta y_{i-1} + B_i \Delta y_i + C_i \Delta y_{i+1} = \Delta C_{p_i} \tag{2}$$

In the general case when the contour discretization points are unevenly spaced, the finite difference formulas applied at any point i on the airfoil upper contour line result in

$$A_i = \frac{\beta_1}{x_i - x_{i-1}} - \frac{2\beta_2}{(x_i - x_{i-1})(x_{i+1} - x_{i-1})} \tag{3}$$

$$B_i = -\beta_0 - \frac{\beta_1}{x_k - x_{k-1}} - \frac{\beta_2}{(x_k - x_{k-1})(x_{k+1} - x_k)} \tag{4}$$

$$C_i = -\frac{2\beta_2}{(x_{i+1} - x_{i-1})(x_{i+1} - x_i)} \tag{5}$$

When finite differencing is applied to any point i on the airfoil lower contour line the result is

$$A_i = \frac{2\beta_2}{(x_{i+1} - x_{i-1})(x_i - x_{i-1})} \tag{6}$$

$$B_i = \beta_0 - \frac{\beta_1}{x_{i+1} - x_i} - \frac{\beta_2}{(x_i - x_{i-1})(x_{i+1} - x_i)} \tag{7}$$

$$C_i = \frac{\beta_1}{x_{i+1} - x_i} - \frac{2\beta_2}{(x_{i+1} - x_i)(x_{i+1} - x_{i-1})} \tag{8}$$

To avoid the ambiguity of the upper and lower contour line finite difference equations, new equations must be defined at the leading and trailing edges of the airfoil:

$$-\Delta y_{i_{LE}-1} + 2\Delta y_{i_{LE}} - \Delta y_{i_{LE}+1} = 0 \tag{9}$$

$$\Delta y_{TE} = 0 \tag{10}$$

These equations form a tri-diagonal system (2), which can easily and efficiently be solved using the Thomas algorithm. One major problem with the classical MGM approach to inverse shape design is its slow convergence at the leading and trailing edges of the airfoil, as compared to the mid-chord regions of the airfoil. Another major problem is the governing equation's non-physical, *ad hoc* nature. Furthermore, there is no analytical method to determine the optimum coefficients β_0, β_1, β_2 in (1), while their choice can radically change the convergence of the inverse shape design process.

In an attempt to counter these problems while improving the convergence rate of the design process, a new method of solution of the MGM equation has been devised. It is based on the transformation of the x-derivatives in (1) to derivatives with respect to a surface-following coordinate, s. This method uses an analytical solution of the shape evolution equation (1) through a Fourier series formulation.

FOURIER SERIES SOLUTION OF MGM SHAPE EVOLUTION EQUATION

The analytical solution of the MGM equation given in (1) is complicated by the fact that the β_0 and β_2 terms switch signs when moving from the bottom surface of the airfoil to the top surface (or vice versa). If β_0, β_1, β_2 are considered to be positive constants, (1) takes the following forms on the top and bottom surfaces of an airfoil:

Top Surface: $$\beta_0 \Delta y + \beta_1 \frac{d\Delta y}{ds} - \beta_2 \frac{d^2 \Delta y}{ds^2} = \Delta C_p(s) \tag{11}$$

Bottom Surface: $$-\beta_0 \Delta y + \beta_1 \frac{d\Delta y}{ds} + \beta_2 \frac{d^2 \Delta y}{ds^2} = \Delta C_p(s) \tag{12}$$

Both (11) and (12) can be considered as the generalized mass-damper-spring equation

$$m\Delta y_{ss} + c\Delta y_s + k\Delta y = \Delta C_p(s) \tag{13}$$

where the time coordinate has been replaced with the surface following coordinate, s, and the forcing function $\ddot{A}C_p(s)$ is an arbitrary function of the coordinate s. The homogeneous solution of (13) can be found by assuming

$$\Delta y_h = e^{\lambda s} \tag{14}$$

On the bottom surface of the airfoil this leads to

$$k^{bottom} = \beta_0 \tag{15}$$

$$c = \beta_1 \tag{16}$$

$$m^{bottom} = -\beta_2 \tag{17}$$

$$\lambda_{1,2}^{bottom} = \frac{-\beta_1 \pm \sqrt{\beta_1^{\,2} + 4\beta_0\beta_2}}{-2\beta_2} \tag{18}$$

$$\Delta y_h^{bottom} = F^{bottom} e^{\lambda_1^{bottom} s} + G^{bottom} e^{\lambda_2^{bottom} s} \tag{19}$$

On the top surface of the airfoil this leads to

$$k^{top} = -\beta_0 \tag{20}$$

$$m^{top} = \beta_2 \tag{21}$$

$$\lambda_{1,2}^{top} = \frac{-\beta_1 \pm \sqrt{\beta_1^{\,2} + 4\beta_0\beta_2}}{2\beta_2} \tag{22}$$

$$\Delta y_h^{top} = F^{top} e^{\lambda_1^{top} s} + G^{top} e^{\lambda_2^{top} s} \tag{23}$$

where F and G are (as yet) undetermined coefficients. The particular solution of (13) can be found by creating a Fourier series expansion of the function $\Delta C_p(s)$ such as

$$\Delta C_p(s) = a_0 + \sum_n [a_n \cos N_n s + b_n \sin N_n s] \tag{24}$$

where

$$N_n = \frac{n\pi}{L} \tag{25}$$

Here, L is one-half of the total arc length of the airfoil contour. A particular solution is assumed of the form

$$\Delta y_p = A_0 + \sum_{n=1}^{\infty} [A_n \cos N_n s + B_n \sin N_n s] \tag{26}$$

Then,

$$\Delta y_p' = \sum_{n=1}^{\infty} [-A_n N_n \cos N_n s + B_n N_n \sin N_n s] \tag{27}$$

$$\Delta y_p'' = -\sum_{n=1}^{\infty} [A_n N_n^2 \cos N_n s + B_n N_n^2 \sin N_n s] \tag{28}$$

Substitution of (24) and (26-28) into the general evolution equation (13) and collection of like terms yields

$$A_0 = \frac{a_0}{k} \tag{29}$$

$$A_n = \frac{a_n(k - N_n^2 m) - b_n(cN_n)}{(k - N_n^2 m)^2 + (cN_n)^2}, \; n = 1,2,3,\cdots \tag{30}$$

$$B_n = \frac{b_n(k - N_n^2 m) + a_n(cN_n)}{(k - N_n^2 m)^2 + (cN_n)^2}, \; n = 1,2,3,\cdots \tag{31}$$

Thus, the complete solution for Δy on the top or bottom surface of the airfoil is

$$\Delta y = Fe^{\lambda_1 s} + Ge^{\lambda_2 s} + A_0 + \sum_{n=1}^{\infty}\left[A_n \cos N_n s + B_n \sin N_n s\right] \tag{32}$$

The unknown constants, F and G, on the top and bottom surfaces are determined by specifying four boundary conditions. In this study, the following four conditions were used: trailing edge closure, leading edge closure, zero trailing edge displacement, and smoothness of Δy at the leading edge. For trailing edge closure,

$$\Delta y^{bottom}(0) = \Delta y^{top}(2L) \tag{33}$$

For pinned trailing edge,

$$\Delta y^{bottom}(0) = 0 \tag{34}$$

The combination of (24) and (25) yields the following boundary condition equations:

$$F^{bottom} + G^{bottom} = -\sum_{n=0}^{\infty} A_n^{bottom} \tag{35}$$

$$F^{top} e^{2L\lambda_1^{top}} + G^{top} e^{2L\lambda_2^{top}} = -\sum_{n=0}^{\infty} A_n^{top} \tag{36}$$

For leading edge closure,

$$\Delta y^{bottom}(s_{LE}) = \Delta y^{top}(s_{LE}) \tag{37}$$

$$F^{bottom} e^{s_{LE}\lambda_1^{bottom}} + G^{bottom} e^{s_{LE}\lambda_2^{bottom}} - F^{top} e^{s_{LE}\lambda_1^{top}} - G^{top} e^{s_{LE}\lambda_2^{top}} = \Delta y_p^{top}(s_{LE}) - \Delta y_p^{bottom}(s_{LE}) \tag{38}$$

For smooth leading edge deformation,

$$\frac{d}{ds}\Delta y^{bottom}(s_{LE}) = \frac{d}{ds}\Delta y^{top}(s_{LE}) \tag{39}$$

$$F^{bottom}\lambda_1^{bottom} e^{s_{LE}\lambda_1^{bottom}} + \lambda_2^{bottom} G^{bottom} e^{s_{LE}\lambda_2^{bottom}} - F^{top}\lambda_1^{top} e^{s_{LE}\lambda_1^{top}} - G^{top}\lambda_2^{bottom} e^{s_{LE}\lambda_2^{top}} = \Delta y_p^{top\,\prime}(s_{LE}) - \Delta y_p^{bottom\,\prime}(s_{LE}) \tag{40}$$

F and G coefficients can be found by simultaneous solution of (35), (36), (38), and (40):

$$\begin{Bmatrix} F^{bottom} \\ G^{bottom} \\ F^{top} \\ G^{top} \end{Bmatrix} = \begin{bmatrix} 1 & 1 & 0 & 0 \\ 0 & 0 & e^{2L\lambda_1^{top}} & e^{2L\lambda_2^{top}} \\ e^{s_{LE}\lambda_1^{bottom}} & e^{s_{LE}\lambda_2^{bottom}} & -e^{s_{LE}\lambda_1^{top}} & -e^{s_{LE}\lambda_2^{top}} \\ \lambda_1^{bottom} e^{s_{LE}\lambda_1^{bottom}} & \lambda_2^{bottom} e^{s_{LE}\lambda_2^{bottom}} & -\lambda_1^{top} e^{s_{LE}\lambda_1^{top}} & -\lambda_2^{top} e^{s_{LE}\lambda_2^{top}} \end{bmatrix}^{-1} \cdot \begin{Bmatrix} -\sum_{n=0}^{\infty} A_n^{bottom} \\ -\sum_{n=0}^{\infty} A_n^{top} \\ \Delta y_p^{top\,\prime}(s_{LE}) - \Delta y_p^{bottom\,\prime}(s_{LE}) \\ \Delta y_p^{top\,\prime}(s_{LE}) - \Delta y_p^{bottom\,\prime}(s_{LE}) \end{Bmatrix} \tag{41}$$

This form of the solution of the MGM equation has several advantages over the standard finite difference approach. First, it removes the necessity for an artificial leading edge condition (9) to be generated within the finite difference scheme. Second, any errors due to finite differencing are removed, since the formulation is exact. Finally, it is more easily applicable to the three-dimensional elastic membrane inverse shape design. Because an infinite number of terms of the Fourier series cannot be considered, one must effectively enforce a finite upper limit on the frequency allowed in the y-coordinate deformation.

NUMERICAL RESULTS

The non-linearity of flow-field governing equations, such as Euler and Navier-Stokes equations, has been suspected to cause problems with the speed of MGM convergence [1-6]. To clarify this issue, three flow-field analysis codes have been used in conjunction with the original MGM and the Fourier series method. The three flow-field analysis codes were: a potential flow code with compressibility correction, an Euler compressible flow code, and a compressible viscous flow Navier-Stokes code with a Baldwin-Lomax turbulence model. The initial geometry was a NACA0009 symmetric non-lifting airfoil at free stream Mach number M = 0.5. The target pressure distribution corresponded to the flow-field around NACA0012 non-lifting airfoil at M = 0.5 obtained with each of the three respective flow-field analysis codes.

Figure 1 demonstrates a quick convergence of the airfoil shape and the surface pressure coefficient distribution towards target values in the case of the MGM method and a surface panel code. A very similar convergence rate can be observed when the Fourier series method is used with the panel code (Fig. 2). Similar trends are evident when the Euler flow solver is used with the MGM (Fig. 3) and the Fourier series method (Fig. 4). When a Navier-Stokes code is used as a flow-field solver, the MGM (Fig. 5) and the Fourier series method (Fig. 6) again offer seemingly comparable performances.

When the target surface pressure coefficient distribution was changed to the one corresponding to a cambered lifting NACA1311 airfoil, the two inverse design methods performed with differing reliability for each of the three flow-field analysis codes (Fig. 8). As an example, Fourier series method with the Navier-Stokes flow solver performed the best in the case of the lifting (asymmetric) target surface pressure distribution (Fig. 7 and Fig. 8). Composite plots of convergence histories (Fig. 8) of the MGM method and the Fourier series method with each of the three flow-field analysis codes demonstrate that the Fourier series method converges faster than the original MGM method for lifting and especially for non-lifting airfoil shapes.

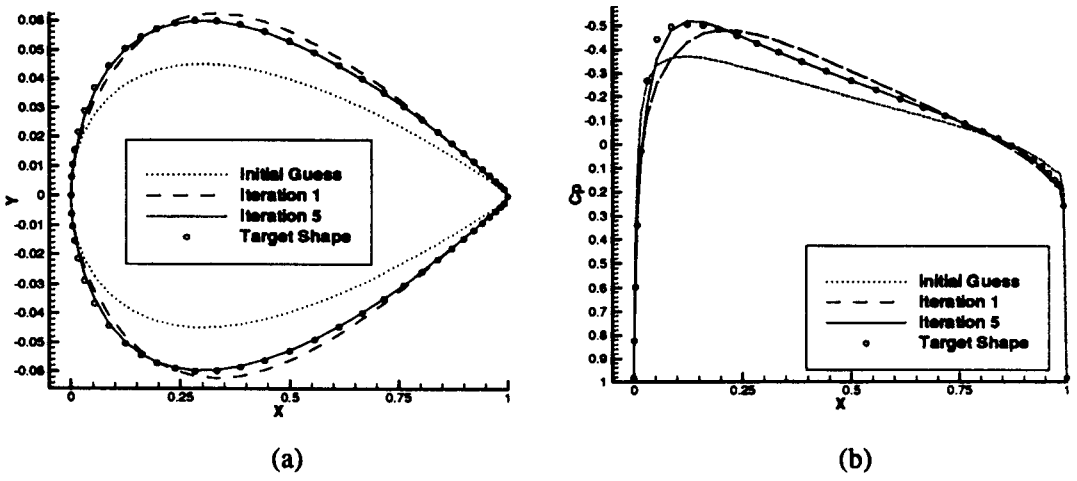

Fig. 1. MGM method: evolution from NACA 0009 to NACA 0012 airfoil. Potential flow solver with Laitone compressibility correction. M=0.5. Beta=(1.2, 0.0, 0.4).
(a) Evolution of geometry. Y-axis enlarged 9 times for clarity.
(b) Evolution of surface coefficient of pressure.

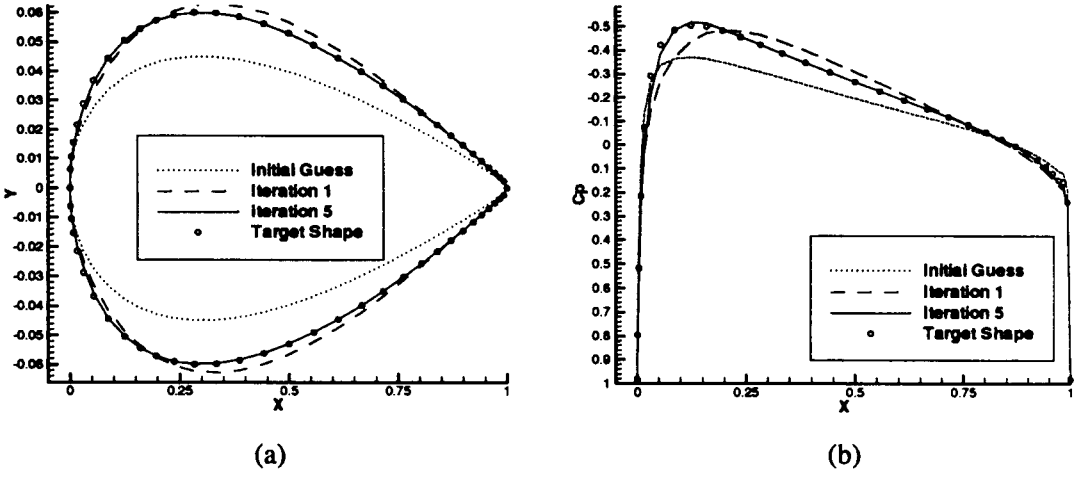

Fig. 2. Fourier method: evolution from NACA 0009 to NACA 0012 airfoil. Potential flow solver with Laitone compressibility correction. M=0.5. Beta=(1.2, 0.0, 0.4).
(a) Evolution of geometry. Y-axis enlarged 9 times for clarity.
(b) Evolution of surface coefficient of pressure.

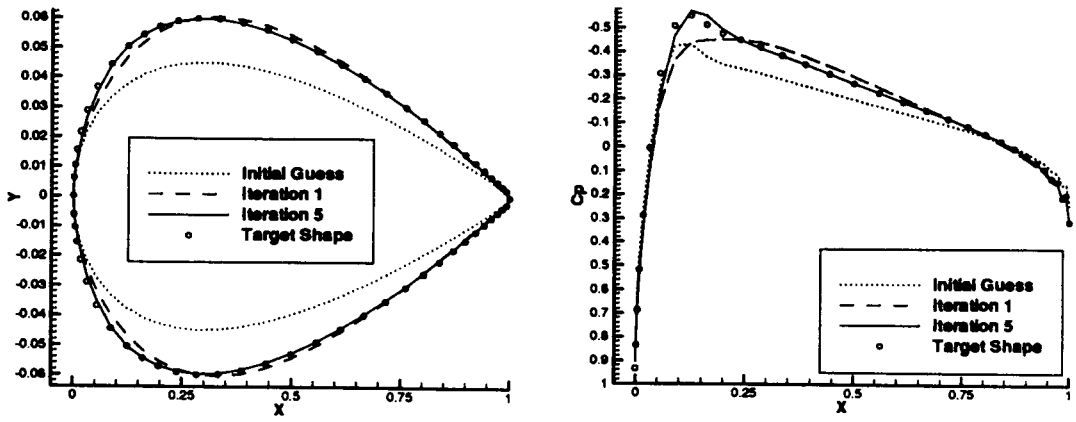

Fig. 3. MGM method: evolution from NACA 0009 to NACA 0012 airfoil. Euler solver. M=0.5. Beta=(1.2, 0.0, 0.4).
(a) Evolution of geometry. Y-axis enlarged 9 times for clarity.
(b) Evolution of surface coefficient of pressure.

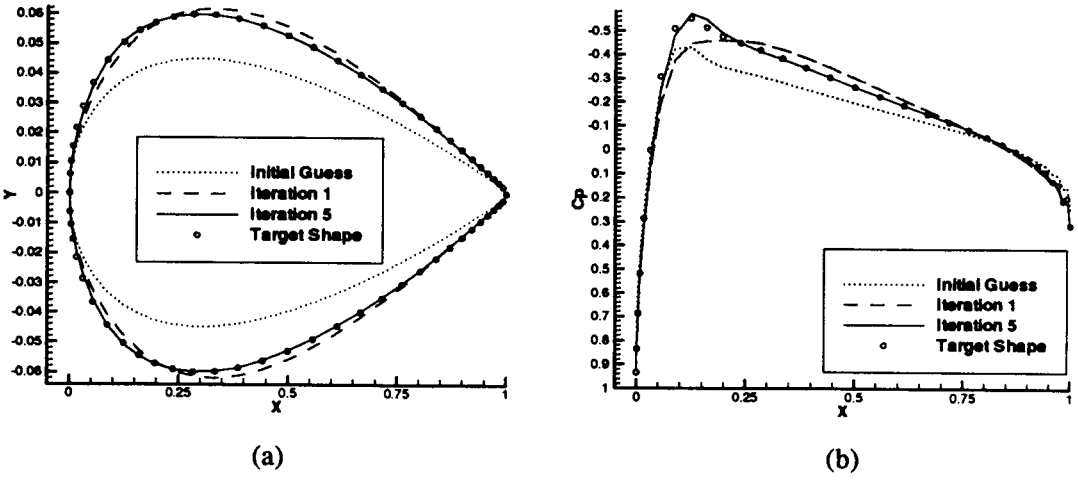

Fig. 4. Fourier method: evolution from NACA 0009 to NACA 0012 airfoil. Euler solver. M=0.5. Beta=(1.2, 0.0, 0.4).
(a) Evolution of geometry. Y-axis enlarged 9 times for clarity.
(b) Evolution of surface coefficient of pressure.

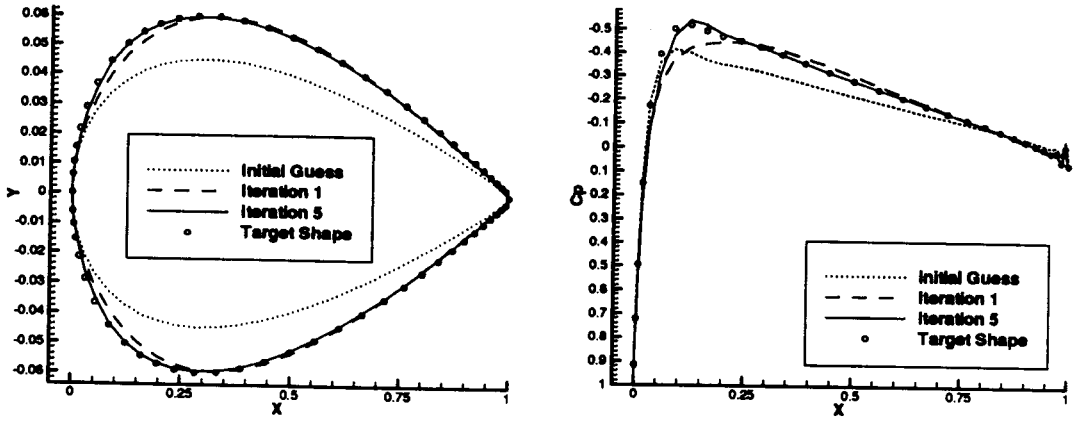

Fig. 5. MGM method: evolution from NACA 0009 to NACA 0012 airfoil. Navier Stokes solver. M=0.5. Beta=(1.2, 0.0, 0.4).
(a) Evolution of geometry. Y-axis enlarged 9 times for clarity.
(b) Evolution of surface coefficient of pressure.

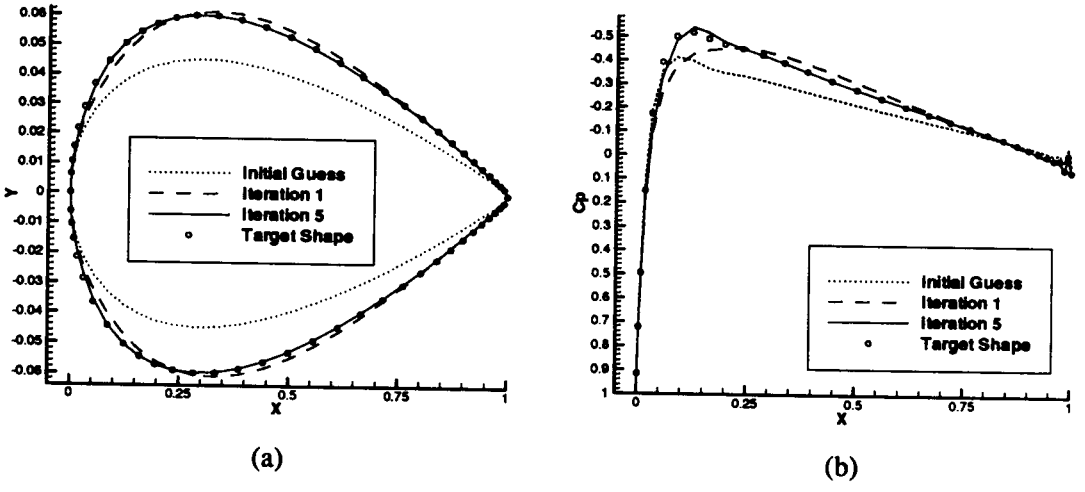

Fig. 6. Fourier method: evolution from NACA 0009 to NACA 0012 airfoil. Navier Stokes solver. M=0.5. Beta=(1.2, 0.0, 0.4).
(a) Evolution of geometry. Y-axis enlarged 9 times for clarity.
(b) Evolution of surface coefficient of pressure.

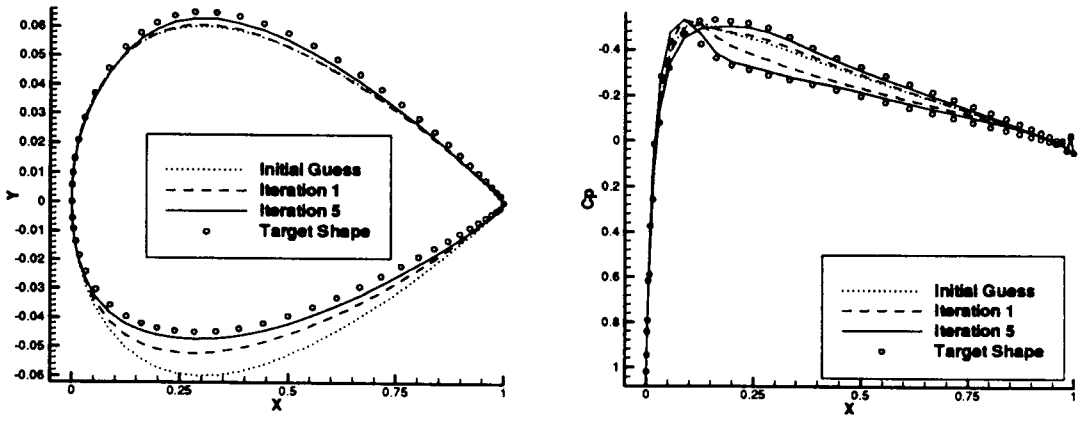

Fig. 7. Fourier method: evolution from NACA 0012 to NACA 1311 airfoil. Navier Stokes solver. M=0.5. Beta=(1.4, 0.0, 0.6).
(a) Evolution of geometry. Y-axis enlarged 9 times for clarity.
(b) Evolution of surface coefficient of pressure.

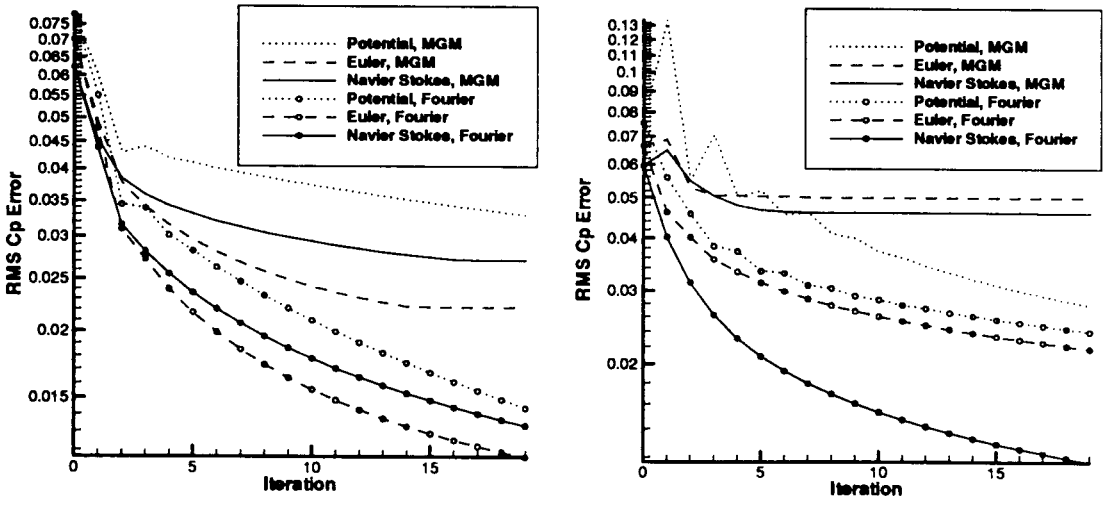

Fig. 8. Convergence histories of MGM and Fourier methods applied to identical problems M=0.5. Re=100000
(a) Nonlifting case: NACA 0009 evolves into NACA 0012. Beta=(1.2, 0.0, 0.4).
(b) Lifting case: NACA 0012 evolves into NACA 1311. Beta=(1.4, 0.0, 0.6)

CONCLUSIONS

From a detailed numerical testing, it can be concluded that convergence rates of both the MGM method and the Fourier series method do not depend on the non-linearity of the flow-field solver used. The Fourier series method was found to consistently converge faster than the MGM method, resulting in fewer calls to the time consuming flow-field solver. Old suspicions that the original MGM method has extremely slow convergence when used with the Navier-Stokes codes has been found to be correct. In the future, it will be possible to formulate and apply the Fourier series method to both two-dimensional and three-dimensional aerodynamic shape inverse designs using any available flow-field analysis code.

ACKNOWLEDGMENTS

The authors would like to express their gratitude for the National Science Foundation Grant DMI-9522854 monitored by Dr. George A. Hazelrigg, the NASA Lewis Research Center Grant NAG3-1995 facilitated by Dr. John K. Lytle and supervised by Dr. Kestutis Civinskas, and for ALCOA Foundation Faculty Research Award facilitated by Dr. Yimin Ruan and Dr. Owen Richmond.

REFERENCES

1. Dulikravich, G.S. (1992). *AIAA J. of Aircraft*, Vol. 29, No. 5, 1020.
2. Dulikravich, G.S. (1995). AIAA Invited Paper 95-0695, Reno, NV.
3. Sobieczky, H. (Ed). (1997). *New Design Concepts for High Speed Air Transport.* Springer, Wien/New York.
4. Garabedian, P. and McFadden, G. (1982). *AIAA J.* Vol.20, No.3, 289.
5. Malone, J.B., Vadyak, J. and Sankar, L.N. (1987). *AIAA J. of Aircraft*, Vol.24, No.1, 8.
6. Malone, J.B., Narramore, J.C., and Sankar, L.N. (1989). In: *AGARD Specialists' Meeting on Computational Methods for Aerodynamic Design (Inverse) and Optimization*, J. Sloof, (Ed). AGARD-CP-463.

INVERSE PROBLEMS IN ENGINEERING MECHANICS

International Symposium on Inverse Problems
in Engineering Mechanics 1998 (ISIP '98)
Nagano, Japan

Editors

M. Tanaka

Department of Mechanical Systems Engineering
Shinshu University, 500 Wakasato, Nagano 380-8553
Japan

G.S. Dulikravich

Department of Aerospace Engineering
The Pennsylvania State University, University Park
PA 16802, USA

1998

ELSEVIER

Amsterdam · Lausanne · New York · Oxford · Shannon · Singapore · Tokyo